MOLECULAR IMAGING AND BIOLOGY

Mol Imaging Biol (2019) 21:669–675
DOI: 10.1007/s11307-018-1282-z

Published Online: 2 October 2018

RESEARCH ARTICLE

Monitoring the Progression of Chronic Liver Damage in Rats Using [^{18}F]PBR06

Shuo Huang, Chao Li, Jun Guo, Linlin Zhang, Shuqi Wu, Hui Wang, Sheng Liang

Department of Nuclear Medicine, Xin Hua Hospital Affiliated To Shanghai Jiao Tong University School, No. 1665, Kongjiang Street, Yangpu District, Shanghai, 200092, China

Abstract

Purpose: Accurate and rapid assessment of liver condition is the key to therapy for hepatitis patients. This study aim is to evaluate the peripheral benzodiazepine receptor (PBR) radioligand [^{18}F]*N*-fluoroacetyl-*N*-(2,5-dimethoxybenzyl)-2-phenoxyaniline ([^{18}F]PBR06) as a positron emission tomography (PET) imaging tracer of chronic liver damage in a rat model.

Procedures: A rat model of liver damage was made by bile duct ligation (BDL), which initiates a complex cascade of pathological events that leads to cholestasis and inflammation, eventually resulting in a severe fibrotic and severe hepatocyte injury. PET scanning, immunofluorescence staining, H&E staining, Masson's staining, and Quantitative real time polymerase chain reaction(qRT-PCR) were performed to elucidate the correlation among the expression level of PBR, radioactivity uptake, and the level of liver damage in the rat model of chronic inflammatory.

Results: Alanine aminotransferase (ALT), aspartate aminotransferase (AST), and total bilirubin (TBIL) increased after BDL and peaked in 1 week, then gradually decreased over the following 3 weeks, although still higher than that of control (all $P < 0.05$). Histological analysis demonstrated chronic severe damage in rat livers after BDL. The uptake of [^{18}F]PBR06 increased in livers and was correlated with severity of liver damage. Further, the mRNA level of PBR was obviously higher compared to controls.

Conclusions: [^{18}F]PBR06 can serve as a sensitive probe to monitor the progression of inflammation in liver. [^{18}F]PBR06 imaging may be used to accurately assess liver damage degree and guide the therapeutic schedule, especially for those patients with severe liver inflammation and damage but with normal or mildly elevated serum ALT and AST. As a non-invasive diagnostic application, [^{18}F]PBR06 PET scan could be an alternative for patients who is unwilling to perform liver biopsy.

Key Words: [^{18}F]PBR06, Positron emission tomography, Inflammation, Liver damage, PBR

Introduction

It is well known that chronic hepatitis may gradually progress to cirrhosis and cancer. Accurately accessing inflammation and injury in liver is the key to formulating effective therapeutic plans. At present, testing the liver function with the level of alanine aminotransferase (ALT) and aspartate aminotransferase (AST) is the most common clinical method. Elevated ALT and AST are usually the indicators of liver injury and are important reference for physicians making decisions [1]. However, the serum ALT and AST level in some progressive hepatitis patients might be normal or only mildly elevated [2]. Moreover, common imaging techniques such as X-ray computed tomography (CT) and magnetic resonance imaging (MRI) have their limitations [3]. For example, there are no specific imaging features for mild

Shuo Huang and Chao Li contributed equally to this work.

Correspondence to: Hui Wang; *e-mail:* Wanghui@xinhuamed.com.cn, Sheng Liang; *e-mail:* liangsheng364214@163.com

liver damage. Liver biopsy is necessary at most time, although it is difficult to be accepted by all patients because of its invasiveness [4]. Therefore, a new non-invasive approach which can be used to accurately and rapidly assess the severity of liver damage has become an urgent issue.

Peripheral benzodiazepine receptor (PBR), also known as the 18-kDa translocator protein (TSPO), is mainly located on the outer mitochondrial membrane and has many biological functions such as anion transport, cell proliferation, apoptosis, cholesterol transport, and immunomodulation. PBR is now known to be widespread in many peripheral organs but expression is much lower in normal brain and liver [5]. Multiple studies have identified that the level of PBR increased markably under many disorder conditions in brain. PBR radioligands for positron emission tomography (PET)/CT have also been used for the non-invasive and reliable assessment of neuropathological damages in experimental animals and human [5–7].

The *N*-[^{18}F]fluoroacetyl-*N*-(2,5-dimethoxybenzyl)-2-phenoxyaniline ([^{18}F]PBR06) is a specific imaging agent for PBR [8]. Because of many advantages, such as ease of preparation, the longer half-life of F-18, insignificant defluorination, high diffusibility across the blood-brain barrier in monkey, high binding affinity for PBR in rat and monkey, and high specificity for PBR, [^{18}F]PBR06 is more promising as compared to the current other PBR radioligands [9]. Also, [^{18}F]PBR06 can been used as a PET imaging agent for neuroinflammatory diseases [9]. To date, [^{18}F]PBR06 PET/CT imaging has not been used in liver yet. Xie *et al*. reported that injured hepatocytes and CD11b + macrophages overexpressed PBR in non-alcoholic fatty liver [10]. Thus, [^{18}F]PBR06 could be used as a potential imaging marker for non-invasive assessment of inflammation and damage in liver.

In this study, we aimed to evaluate [^{18}F]PBR06 as a PET imaging tracer of liver injury in a rat model. To this end, we made rat models of liver damage by bile duct ligation (BDL). PET scanning, immunofluorescence staining, H&E staining, Masson's staining, and Quantitative real time polymerase chain reaction (qRT-PCR) were performed to elucidate the correlation among the expression level of PBR, radioactivity uptake, and the level of liver damage in the rat model of chronic inflammatory. We demonstrated the feasibility of [^{18}F]PBR06 as an imaging biomarker for non-invasive assessment inflammation and damage in liver.

Materials and Methods

Preparation of [^{18}F]PBR06

[^{18}F]PBR06 was synthesized *via* nucleophilic aliphatic substitution and was purified with reversed-phase high-performance liquid chromatography as Wang *et al*. [11]. The specific activity was 47.1 ± 21 GBq/μmol at the time of injection with a non-decay-corrected radiochemical yield of 23.8 % ± 2.32 %.

Preparation of a Rat Model of Chronic Liver Damage

All protocols of animal experiment were approved by the local Animal Experimental Ethics Committee of Xinhua Hospital, Medical School of Shanghai Jiaotong University, Shanghai, China. A total of 30 SD male rat, aged 8 weeks, were maintained in stationary temperature and controlled humidity chambers. The rats were randomly assigned to five groups of six rats each. One group acted as a control group and the other four groups were studied at 1, 2, 3, and 4 weeks after BDL.

Bile Duct Ligation

The rats were maintained under anesthesia by using 2 % isoflurane for the entire procedure. In a sterile environment, a 2-cm midline incision was performed at upper abdomen and the common bile duct was divided and ligated twice [12, 13]. The ligatures were placed at the same position in all animals. With a similar operation, the bile ducts in sham group rats were divided but not ligated.

PET Study on Rats

PET scans were performed by using a small-animal Inveon PET scanner (Siemens Healthcare GmbH, Erlangen, Germany), which provides those parameters: slice thickness = 0.78 mm, matrix size = 128 × 128, field of view (FOV) = 4 × 4 cm^2, energy levels of acquisition 350~650 keV [14]. Rats were anesthetized with isoflurane gas (5.0 % for induction and 1.0–2.0 % for maintenance). Thirty minutes after injection of [^{18}F]PBR06 (average 10 MBq/0.2–0.3 ml), dynamic images were acquired. All images were reconstructed by using a three-dimensional ordered subset expectation maximum algorithm (3D OSEM). Region of interest (ROI) in liver was drawn automatically avoiding the effect of aortaventralis. The regional uptake of radioactivity was calculated for each ROI and expressed as the standardized uptake value (SUV), which equals radioactivity per milliliter tissue/injected radioactivity × gram body weight. Values of area under of liver ($AUC_{0–30\ min}$, SUV × min) were calculated from 0 to 30 min after injection.

Analysis of Liver Enzymes in Serum

The five per group rats were euthanized by exsanguination under chloral hydrate anesthesia at weeks 1, 2, 3, and 4 after PET/CT scans. The blood was collected and kept at room temperature (RT) for 2 h, followed by centrifugation at 12000 rpm for 10 min to obtain sera. The biochemical indicators of liver function, including ALT, AST, and total bilirubin (TBIL) were measured by corresponding kits (Nanjing Jiancheng Bioengineering Institute, China) [14].

Histopathology Assay

After measuring the weight of the whole liver, liver samples were immersed in 4 % paraformaldehyde for 48 h. The left and right liver lobes were placed in wide-mouth bottle, dehydrated through a serial alcohol gradient, and embedded in paraffin wax blocks. The specimens were serially sectioned to provide 4-μm thick liver tissue sections, then dewaxed in xylene, rehydrated through decreasing concentrations of ethanol, and washed in PBS. The tissue sections were stained with H&E and Masson's staining according to the manufacturer's protocols and observed under a light microscope.

Immunohistochemical Staining Assay

The paraffin was removed from the sections (5.0-μm thickness) following routine methods and then incubated in buffered normal goat serum to prevent nonspecific binding of antibodies for 1 h at RT. Then, liver sections were incubated separately overnight with antibodies against PBR (ab154878, Abcam, 1:200), followed by incubation with CY3-conjugated goat anti-rabbit IgG (GB21303; dilution 1:300; Servicebio) for 1 h at 37 °C. Thereafter, the sections were washed in PBS. 4,6-Diamidino-2-phenylindole (DAPI) was used to stain the cell nuclei (blue) at a concentration of 1 μg/ml (G1012; Servicebio). Photomicrographs were taken with a DMI3000B camera (Leica).

Real-time Polymerase Chain Reaction

Total RNA was extracted from frozen livers using Trizol reagent (9109; Takara, Liaoning, China) according to the manufacture's protocol. The quality of total RNA was checked by measuring the ratio of absorbance at 260/280 nm with a NanoDrop ND-1000 (LMS, Tokyo). The RNA then was reverse-transcribed into cDNA using the PrimeScript RT Master Mix kit (RR036A; Takara). cDNA were used as template for quantitative real-time PCR using the SYBR Premix Ex TaqTM kit (RR420A; Takara) with an ABI PRISM 7500 real-time PCR system (Applied Biosystems, Foster, California, USA). Target-specific primers for the target gene (PBR) were purchased from Applied Biosystems. The amount of PBR was normalized to the amount of GAPDH cDNA (B661104; Sangon Biotech, Shanghai, China). All amplification reactions were done in triplicate.

Statistics

Quantitative data were expressed as mean ± SE, and the results of each group followed a normal distribution. Statistical analyses of data were performed using Dunnett's or Tukey's tests within GraphPad Prism (version 6.0 d; GraphPad Software Inc.). The correlation of radiotracer uptake data at 4 weeks with the PBR expression levels was analyzed using SPSS (version 17). Image J (version 1.46) was used to analyze immunofluorescence results. The PBR relative expression levels were calculated regarding the PBR positive area%, when P value < 0.05 between groups were considered significant.

Results

Liver Function in Serum

As compared with the control group, BDL group showed significant liver damage (Table 1). The level of AST, ALT, and TBIL increased after BDL and peaked in 1 week, then gradually dropped along with time until 4 weeks, which were still higher than control. At 1 week, the level of ALT (399.79 ± 98.09 IU/l), AST (610.10 ± 110.31 IU/l), and TBIL (104.40 ± 40.36 μmol/l) were 6.6-fold, 8.4-fold, and 19.9-fold higher than that in the control group, respectively.

Histological Analysis

Figures 1 and 2 respectively show H&E-stained images and Masson-stained images. The results indicated the rats after BDL suffer sever liver inflammation and fibrosis. At 2 weeks, we saw that mild inflammatory cells infiltrate around proliferated bile ducts after BDL induction. The expansions of fibrotic tissue into some hepatic lobules were observed. At 3 weeks, mild cholestasis deposited in hepatic cell interstitium. Membrane-like intervals formed in some portal to portal area. Four weeks after BDL, large amounts of bile are deposited in hepatocytes interstitium. Morphological changes and cable arrangement of hepatocytes were observed. Membrane-like intervals connected to each other and formed the pseudolobule. Some rats showed late-stage cirrhosis.

PET Scans

PET/CT scans were performed at 30 min after injection of [^{18}F]PBR06 to visualize liver damage in BDL rats. Figure 3a, b shows the PET images and the time-activity curves in the liver over the 4 weeks of this study. The images show the higher uptake of [^{18}F]PBR06 in the rat

Table 1. Comparisons of ALT, AST, and TBIL measurements

	n	TBIL (μmol/l)	ALT (U/l)	AST (U/l)
Control	6	5.23 ± 1.12	60.21 ± 13.2	71/93 ± 23.4
1 week	5	104.4 ± 40.4*	399.8 ± 98.1*	610.1 ± 110*
2 weeks	6	80.43 ± 23.9*	236.5 ± 81.2*	410.4 ± 138*
3 weeks	5	48.64 ± 15.4*	152.4 ± 36.3*	265.3 ± 94.4*
4 weeks	6	14.83 ± 4.21*	69.87 ± 14.8	78.57 ± 15.4

Data are represented as the mean ± SE. *$P < 0.05$

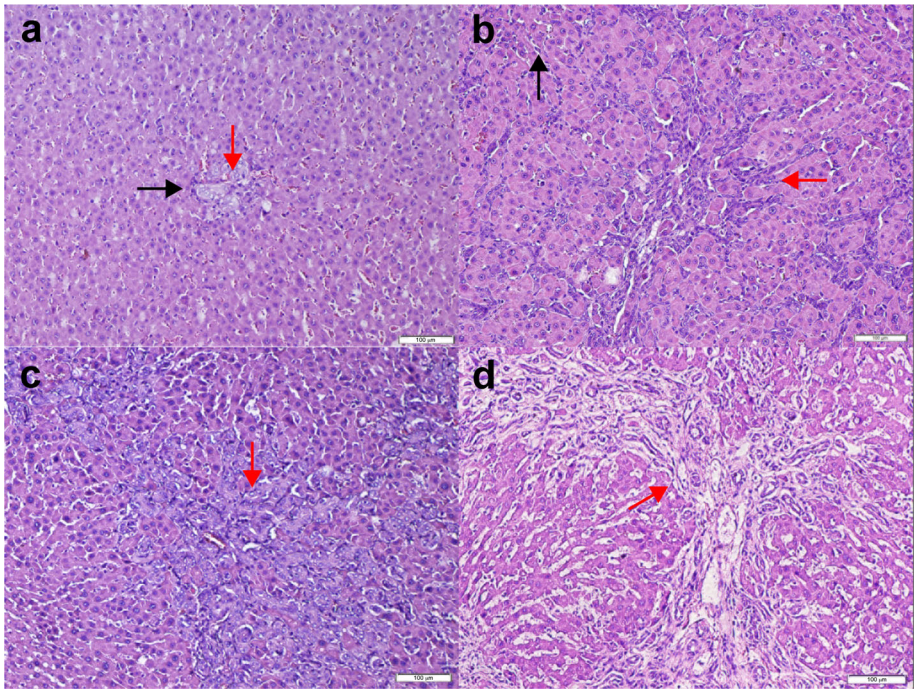

Fig. 1 H&E-stained images **a** at 1 week: sprinkling of inflammatory cells (black arrows) infiltrated around mild hyperplastic bile ducts (red arrows); **b** at 2 weeks: increased inflammatory cells (black arrows) infiltrated in hepatic cells interstitium. Marked proliferated biliary epithelial cells expanded into hepatic lobules (red arrows); **c** at 3 weeks: mild cholestasis deposited in hepatic cells interstitium. Membrane-like intervals formed in portal to portal area (red arrows); and **d** at 4 weeks: large amounts of bile are deposited in hepatocytes interstitial. Morphological changes and cable arrangement of hepatocyte were observed. Membrane-like intervals connected to each other and formed the pseudolobule (red arrows).

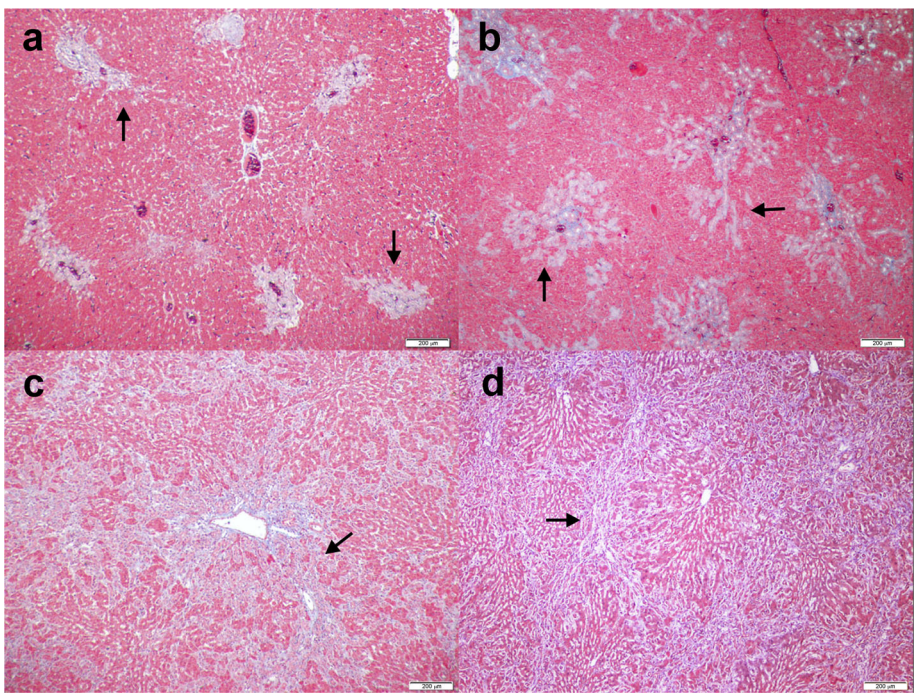

Fig. 2 Masson-stained images **a**, **b** at 1–2 weeks. Biliary epithelial cells proliferated mildly and expanded into some hepatic lobules (black arrows); **c** at 3 weeks: perivascular and pericellular fibrosis developed with marked bridging (black arrows); and **d** at 4 weeks: membrane-like intervals connected to each other and formed the pseudolobule (black arrows).

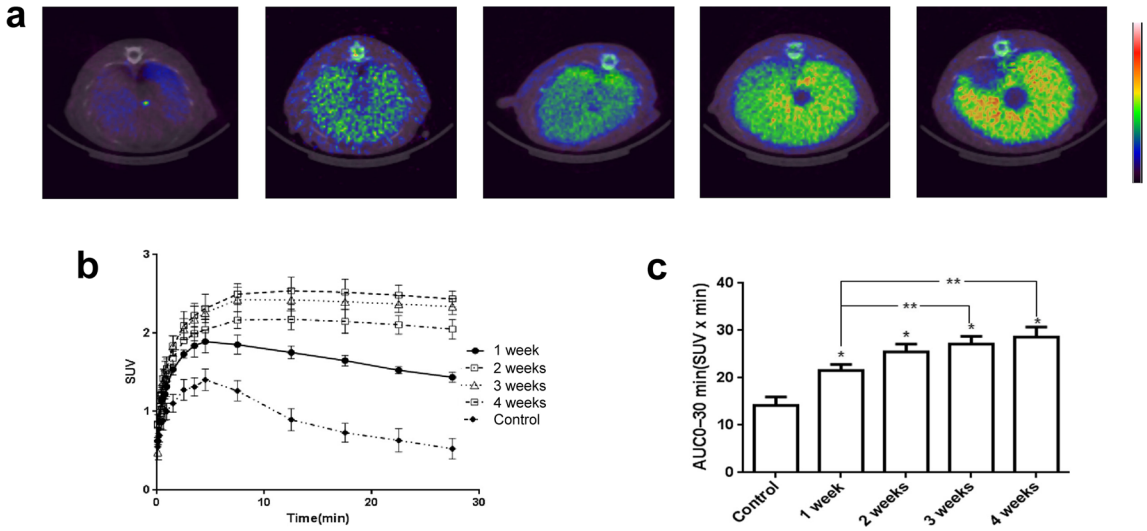

Fig. 3 **a** Representative coregistered PET/CT fusion images of rat livers after injection of [18F]PBR06. **b** Time-activity curves of [18F]PBR06 in the livers from 0 to 30 min after injection. **c** Radioactivity values ($AUC_{0–30\ min}$, SUV × min, mean ± SE) calculated from the time-activity curves between 0 and 30 min. *$P < 0.0001$ for control *versus* 1, 2, 3, or 4 weeks after BDL. **$P < 0.0001$ for 1 weeks after BDL *versus* 3 or 4 weeks.

liver of BDL groups, as compared to control group. Additionally, radioactivity in the livers gradually increased along with disease progression after BDL. Consistent with the PET images, the time-activity curves show the accumulating of radioactivity in the livers increased significantly 1–3 weeks after BDL and reached a maximum at 4 week. Figure 3c shows the uptake value, represented as the area under the time-activity curves ($AUC_{0–30\ min}$), in the livers. The values of 1 week, 2 weeks, 3 weeks, and 4 weeks in the BDL groups were 21.6 ± 1.2 (1.5 fold), 25.5 ± 1.6 (1.8 fold), 27.1 ± 1.6 (1.9 fold), and 28.7 ± 2.0 (2.0 fold), respectively, compared to the control group (14.1 ± 1.8) ($P < 0.0001$).

PBR Expression in Liver

To study the expression of PBR in liver and confirm the PET/CT results, immunofluorescence staining was performed. Figure 4 shows PBR (red) which appeared to be mainly localized in the cytoplasm and occasionally the nucleus in hepatocyte. In the control group, the normal hepatocyte showed no or low expression of PBR. In the BDL groups, the level of PBR expression significantly increased with disease progression and hepatocellular injury. Our results identified PBR preferentially localized at the lesion sites in injured hepatocytes. A close correlation between radiotracer uptake data with the PBR expression levels was observed (Pearson's $r = 0.831$, $P = 0.000$, Fig. 5).

PBR mRNA Expression

Finally, we used qRT-PCR to quantify the mRNA level of PBR (Fig. 6). The expression level of PBR mRNA expression was increased at 1 week (1.9-fold), 2 weeks (2.3-fold), 3 weeks (3.4-fold), and 4 weeks (3.7-fold) after BDL, comparing with the control group ($P < 0.05$). This result further confirmed the above findings. It suggests that the PBR mRNA is correlated with the level of liver damage.

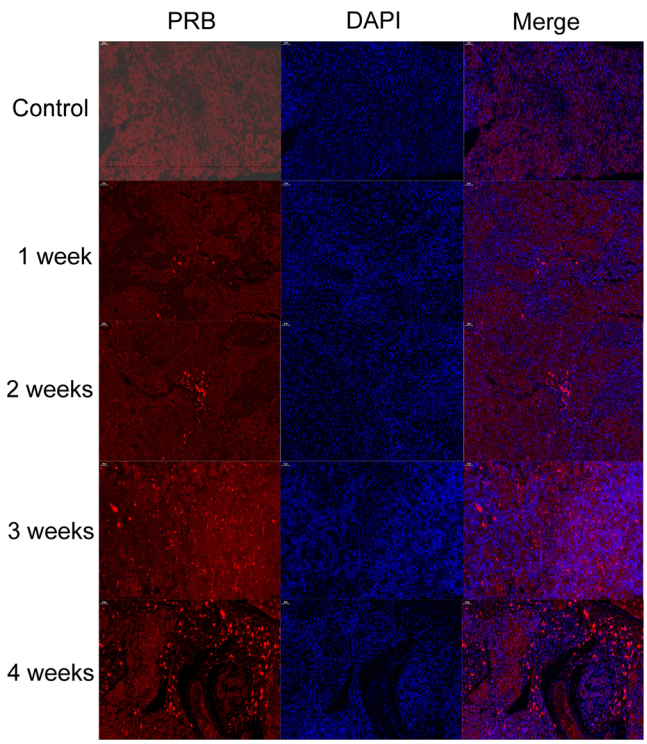

Fig. 4 Immunofluorescence staining of PBR (red) and DAPI (blue).The level of PBR expression significantly increased with disease progression and hepatocellular injury.

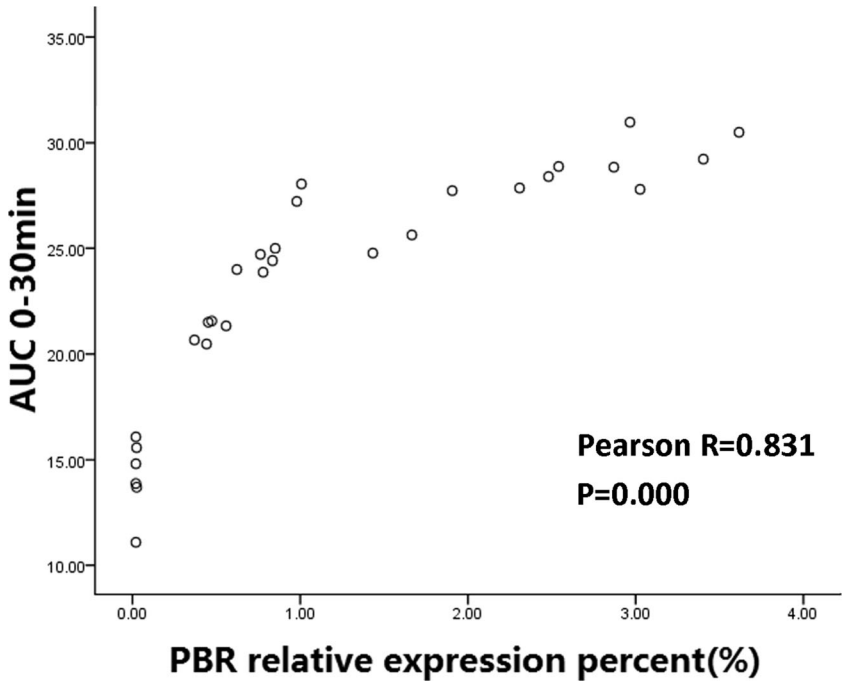

Fig. 5 Correlation between radiotracer uptake data with the PBR expression levels (Pearson's $r = 0.831$, $P = 0.000$). The PBR relative expression percent was calculated regarding the PBR positive area%.

Discussion

To our knowledge, this is the first time that [18F]PBR06, as a reliable radioligand for neuroinflammation disease, is used to directly visualize chronic hepatocellular injury. Chronic liver damage is a common clinical disease. Testing serum ALT and AST is a first-line screening procedure for it. However, some patients with serious liver damage have normal or mildly elevated serum ALT and AST [2]. Imaging methods are also commonly used in clinical practice, but there are limitations in accurately and rapidly distinguishing liver damage and assessing damage severity [3]. At this time, liver biopsy, the gold standard of liver disease, is often necessary to confirm the true condition of patients' liver. Because of many disadvantages, such as pain, complications, and false negative due to sampling errors, not all patients are willing to undergo liver biopsy [4]. Therefore, non-invasive methods with higher accuracy and less inclined to sampling errors are needed to provide complementary information for diagnoses and monitoring.

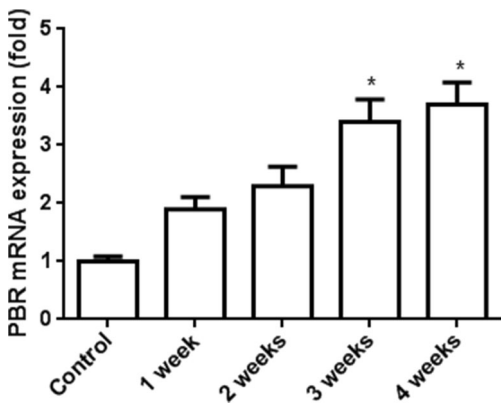

Fig. 6 Expression of hepatic PBR mRNA in control rats and rats after BDL for 1, 2, 3, or 4 weeks. *$P < 0.05$ for the control *versus* 3 or 4 weeks after BDL.

Rats subjected to BDL could have excessive accumulation of hydrophobic bile acids and infiltration of inflammatory cells such as macrophages, monocytes, and lymphocytes, which are considered as the main cause of strong fibrosis and severe hepatocellular injury [15]. The results of H&E and Masson's staining show the gradually aggravated liver pathological damage. Progressive liver damage is further confirmed by elevated serum activities of AST, AST, and TBIL, which peaked in 1 week. Interestingly, the value of AST, AST, and TBIL then gradually decreased with disease progression. This symptom could be an attribution of hepatic blood perfusion decrease, cholestasis, and inflammatory cell infiltration which impaired synthesizing function of hepatocyte. These results further proved that serum markers, such as ALT and AST, are not reliable indicators for accurate assessment of liver damage.

The images of PET/CT with inflammatory imaging radioligand [18F]PBR06 for the rats 1 week, 2 weeks, 3 weeks, and 4 weeks after BDL show the severity of liver damage in different periods. Comparisons of liver images and $AUC_{0-30\ min}$ values between the control and BDL groups suggested that the levels of radioactivity and radiotracer binding gradually elevated in the livers along with the severity of damage. Four weeks after BDL, although the liver-associated enzymes such as ALT and AST only mildly elevated, the radioactivity in liver significantly increased when compared to that of the control

group. This result proved that [^{18}F]PBR06 may be a more reliable probe for liver damage than ALT and AST.

PBR is known to be widely expressed in peripheral organs including kidney, lung, heart, testis, ovary, and uterus, in particular in the adrenal gland kidney. But the densities in brain and liver is low [5]. Not only did our immunohistochemical staining result further confirm this point, but the results also proved that the expression level of PBR increase with the progression of liver damage. PBR preferentially localized at the cytoplasm and occasionally the nucleus in injury hepatocytes and macrophages in BDL liver. The level of PBR mRNA expression was also consistent with immunohistochemical staining result.

Rats undergoing BDL would accumulate excessive amount of hydrophobic bile acids, which can be deemed as the main cause leading to hepatotoxicity [16]. By them, partial impairment concerning functions of mitochondrial electron transport chain in the liver could be observed [16, 17]. In addition, severe hemodynamic alterations take place in the liver underwent BDL, involving the portal and arterial types, which are influenced by oxidative stress and ischemia/reperfusion. The increase of vascular resistance in the portal system of liver generated from extrahepatic cholestasis will lead to portal hypertension [18, 19] and liver ischemia, while deficient NO and inducible nitric oxide synthase (iNOS) will be produced [20]. Interestingly, PBR is attributed to immune regulation, with elevated expression observed in microglia and macrophages. The overexpression of PBR has also been linked in multiple disorders, including reduced mitochondrial respiration [21] and ischemia/reperfusion injury [22]. Those may be the probable cause of PBR overexpression. Further studies are still required to understand the specific mechanisms.

Conclusion

In summary, [^{18}F]PBR06 can serve as a sensitive probe to monitor the progression of inflammation in liver. [^{18}F]PBR06 imaging may be used to accurately assess liver damage degree and guide the therapeutic schedule, especially for those patients with severe liver inflammation and damage but with normal or mildly elevated serum ALT and AST. As a non-invasive measurement, [^{18}F]PBR06PET scans should be a choice for patients who is unwilling to accept liver biopsy.

Acknowledgements. This work was supported by Department of Nuclear Medicine, Xin Hua Hospital Affiliated to Shanghai Jiao Tong University School and HuaYi Molecular Imaging Institute. We are grateful to the staff of our institute for their technical support and assistance with cyclotron operation, radionuclide production, and animal experiments.

Compliance with Ethical Standards

Conflict of Interest

The authors declare that they have no conflict of interest.

References

1. Lok AS, McMahon BJ (2009) Chronic hepatitis B: update 2009. Hepatology 50:661–662
2. Kumar M, Sarin SK, Hissar S, Pande C, Sakhuja P, Sharma BC, Chauhan R, Bose S (2008) Virologic and histologic features of chronic hepatitis B virus-infected asymptomatic patients with persistently normal ALT. Gastroenterology 134:1376–1384
3. Boll DT, Merkle EM (2009) Diffuse liver disease: strategies for hepatic CT and MR imaging. Radiographics 29:1591–1614
4. Martínez SM, Crespo G, Navasa M, Forns X (2011) Noninvasive assessment of liver fibrosis. Hepatology 53:325–335
5. Gavish M, Bachman I, Shoukrun R, Katz Y, Veenman L, Weisinger G, Weizman A (1999) Enigma of the peripheral benzodiazepine receptor. Pharmacol Rev 51:629–650
6. Liu GJ, Middleton RJ, Hatty CR, Kam WWY, Chan R, Pham T, Harrison-Brown M, Dodson E, Veale K, Banati RB (2014) The 18 kDa translocator protein, microglia and neuroinflammation. Brain Pathol 24:631–653
7. Kannan S, Balakrishnan B, Muzik O, Romero R, Chugani D (2009) Positron emission tomography imaging of neuroinflammation. J Child Neurol 24:1190–1199
8. Briard E, Zoghbi SS, Siméon FG et al (2009) Single-step high-yield radiosynthesis and evaluation of a sensitive ^{18}F-labeled ligand for imaging brain peripheral benzodiazepine receptors with PET. J Med Chem 52:688–699
9. Lartey FM1, Ahn GO, Shen B et al (2014) PET imaging of stroke-induced neuroinflammation in mice using [^{18}F]PBR06. Mol Imaging Biol 16:109–117
10. Xie L, Yui J, Hatori A, Yamasaki T, Kumata K, Wakizaka H, Yoshida Y, Fujinaga M, Kawamura K, Zhang MR (2012) Translocator protein (18 kDa), a potential molecular imaging biomarker for non-invasively distinguishing non-alcoholic fatty liver disease. J Hepatol 57:1076–1082
11. Wang M, Gao M, Miller KD, Zheng QH (2011) Synthesis of [^{11}C]PBR06 and [^{18}F]PBR06 as agents for positron emission tomographic (PET) imaging of the translocator protein (TSPO). Steroids 76:1331–1340
12. Tag CG, Sauer-Lehnen S, Weiskirchen S et al (2015) Bile duct ligation in mice: induction of inflammatory liver injury and fibrosis by obstructive cholestasis. J Vis Exp. https://doi.org/10.3791/52438
13. Abdel-Aziz G, Lebeau G, Rescan PY, Clément B, Rissel M, Deugnier Y, Campion JP, Guillouzo A (1990) Reversibility of hepatic fibrosis in experimentally induced cholestasis in rat. Am J Pathol 137:1333–1342
14. Kong X, Luo S, Wu JR, Wu S, de Cecco CN, Schoepf UJ, Spandorfer AJ, Wang CY, Tian Y, Chen HJ, Lu GM, Yang GF, Zhang LJ (2016) ^{18}F-DPA-714 PET imaging for detecting neuroinflammation in rats with chronic hepatic encephalopathy. Theranostics 6:1220–1231
15. Aller MA, Arias JL, García-Domínguez J et al (2008) Experimental obstructive cholestasis: the wound-like inflammatory liver response. Fibrogen Tissue Repair 1. https://doi.org/10.1186/1755-1536-1-6
16. Poli G (2000) Pathogenesis of liver fibrosis: role of oxidative stress. Mol Asp Med 21:49–98
17. Huang YT, Hsu YC, Chen CJ, Liu CT, Wei YH (2003) Oxidative-stress-related changes in the livers of bile-duct-ligated rats. J Biomed Sci 10:170–178
18. Ohara N, Schaffner T, Reichen J (1993) Structure-function relationship in secondary biliary cirrhosis in the rat. Stereologic and heodynamic characterization of a model. J Hepatol 17:155–162
19. Li T, Yang Z (2005) Research progress of vasculopathy in portal hypertension. World J Gastroenterol 11:6079–6084
20. Baron V, Hernandez J, Noyola M et al (2000) Nitric oxide and inducible nitric oxyde synthase expression are downregulated in acute cholestasis in the rat accompanied by liver ischemia. Comp Biochem Physiol C Toxicol Pharmacol:127, 243–249
21. Gatliff J, East D, Crosby J, Abeti R, Harvey R, Craigen W, Parker P, Campanella M (2014) TSPO interacts with VDAC1 and triggers a ROS-mediated inhibition of mitochondrial quality control. Autophagy 10:2279–2296
22. Casellas P, Galiegue S, Basile AS (2002) Peripheral benzodiazepine receptors and mitochondrial function. Neurochem Int 40:475–486